Inorg. Chem. **2009**, *48*, 2224−2232

Determination of the Metal−Dithiolate Fold Angle in Mononuclear Molybdenum(V) Centers by EPR Spectroscopy

Simon C. Drew*,† and Graeme R. Hanson*

The University of Queensland, Centre for Magnetic Resonance and Centre for Metals in Biology, Queensland 4072, Australia

Received December 8, 2008

The active sites of mononuclear molybdenum-containing enzymes contain a low-symmetry Mo^V−dithiolene intermediate whose structure can be probed using electron paramagnetic resonance (EPR). The relationship between experimental EPR spectra and the electronic and geometric structure of the active site can be difficult to establish, not least because of the low molecular symmetry. When density functional theory is used, it is possible to assess this relationship by systematically varying the geometric structure and comparing the theoretical EPR parameters with those obtained experimentally. We employed this approach to examine the relationship between the metal−dithiolate fold angle and the monoclinic spin Hamiltonian parameters (**g**, **A**, β) of a prototypical mononuclear molybdenyl model complex. By comparing the experimental EPR parameters with these results, we show that the metal−dithiolate fold angle of the complex in solution may be obtained from the non-coincidence angle β that transforms the principal axes of **g** to those of **A**. This will provide a useful method for probing the structure of the Mo^V intermediate of mononuclear molybdenum enzymes, where the electronic structure of the active site is modulated by the fold angle of the dithiolate ligand (the "metal−dithiolate folding effect").

Introduction

Molybdenum enzymes play vital roles in plant, animal, and human health; the carbon, sulfur, and nitrogen cycles; biofeedback systems; and the control of the global climate.[1−5] They typically contain a mononuclear Mo active site coordinated by one or two tricyclic pterin−dithiolene ligands, known as molybdoterin (MPT), together with a complement of oxo, sulfido, water-based, and amino acid ligands. The enzymes cycle through the formal molybdenum oxidation states +6, +5, and +4, where the Mo^V (d^1) intermediate is paramagnetic, and catalyze a variety of net oxygen atom transfer reactions. Electron paramagnetic resonance (EPR) is routinely employed to interrogate the paramagnetic states and provides valuable structural and mechanistic information.[6−9]

MPT has been suggested to play a role in tuning the redox potential of enzyme active sites, controlling the reactivity of coligands, stabilizing the multiple Mo oxidation states, and facilitating electron transfer between the Mo active site and other redox partners.[1−5,10,11] These functions have been linked to a "dithiolate folding effect" involving overlap of the metal in-plane and sulfur−π orbitals upon the folding of the MoS_2C_2 metallacycle along the S−S axis of the MPT ligand.[10,12,13]

* E-mail: sdrew@unimelb.edu.au (S.C.D.), graeme.hanson@cmr.uq.edu (G.R.H.).
† Current address: Department of Pathology, The University of Melbourne, Victoria, 3010, Australia.

(1) Hille, R. *Chem. Rev.* **1996**, *96*, 2757–2816.
(2) Pilato, R. S.; Stiefel, E. I. In *Bioinorganic Catalysis*; Reedijk, J., Bouwman, E., Eds.; Marcel Dekker: New York, 1999; pp 81−152.
(3) Sigel, A.; Sigel, H. *Metal Ions in Biological Systems (Molybdenum and Tungsten: Their Roles in Biological Processes)*; Marcel Dekker: New York, 2002; Vol. *39*.
(4) Tunney, J. M.; McMaster, J.; Garner, C. D. In *Comprehensive Coordination Chemistry II*; McCleverty, J. A., Meyer, T. J., Eds.; Elsevier Pergamon: Amsterdam, 2004; Vol. *8*, Chapter 8.18, pp 459−477.
(5) Young, C. G. In *Encyclopedia of Inorganic Chemistry 2*; King, R. B., Scott, R. A., Eds.; Wiley: Chichester, U. K., 2005.
(6) Kisker, C.; Schindelin, H.; Rees, D. C. *Annu. Rev. Biochem.* **1997**, *66*, 233–67.
(7) Romão, M. J.; Robert, H. In *Structure and Bonding*; Springer Verlag: Berlin, 2004; Vol. *90*, pp 69−95.
(8) Kisker, C.; Schindelin, H.; Baas, D.; Reètey, J.; Meckenstock, R. U.; Kroneck, P. M. H. *FEMS Microbiol. Rev.* **1999**, *22*, 503–521.
(9) Brondino, C. D.; Romão, M. J.; Moura, I.; Moura, J. J. G. *Curr. Opin. Chem. Biol.* **2006**, *10*, 109–114.
(10) Enemark, J. H.; Cooney, J. J. A.; Wang, J.-J.; Holm, R. H. *Chem. Rev.* **2004**, *104*, 1175–1200.
(11) Westcott, B. L.; Gruhn, N. E.; Enemark, J. H. *J. Am. Chem. Soc.* **1998**, *120*, 3382–3386.

10.1021/ic802343f CCC: $40.75
Published on Web 02/04/2009

Molybdenyl ($[Mo^{V}{\equiv}O]^{3+}$) complexes have long been used as structural models for understanding the electronic structure of active sites within mononuclear xanthine oxidase, sulfite oxidase, and nitrate reductase families of molybdenum enzymes.[10] Complexes such as Tp*MoOX (Tp* = hydrotris(3,5-dimethylpyrazol-1-yl)borate; X = benzene-1,2-dithiolate (bdt), toluene-3,4-dithiolate (tdt), and quinoxalinyl-2,3-dithiolate (qdt)) have attracted particular attention.[10,14] Although second-generation true dithiolene complexes (where the ene group does not form part of an aromatic system) of the type Tp*ME{$S_2C_2(CO_2Me)_2$} (M = Mo, W; E = O, S) have also recently been generated,[15] the pseudodithiolene Tp*Mo-
OX complexes remain the most well-defined mononuclear MoO(dithiolene) system.[16] A range of spectroscopic and molecular orbital studies of these complexes has shown that the singly occupied molecular orbital (SOMO) consists of a highly covalent, pseudo-σ interaction between the redox active in-plane Mo orbital and the symmetric combination of dithiolate in-plane sulfur p orbitals.[10]

The EPR spectra of (Tp*)Mo^{V}O(dithiolate) complexes have been described as being essentially identical, with reference to the fact that EPR parameters are primarily determined by the first coordination sphere of the $Mo^{V}O$ center, which is the same for these compounds.[10] However, such assertions place a special emphasis on the principal values of the **g** and **A** interactions while giving lesser consideration to their non-coincidence, which in many cases is nontrivial. We recently studied a series of model complexes including Tp*MoEX (E = O, S; X = bdt) using density functional theory (DFT) and multifrequency EPR.[17,18] From the behavior of the computed electron Zeeman (**g**) and the ^{95}Mo nuclear hyperfine (**A**) matrices, it became apparent that the angle defining the non-coincidence of their principal components in the molecular symmetry plane, β, might be related to the Mo−dithiolate fold angle, η, defined by the dihedral angle between the MoS_2 and S_2C_2 planes (Figure 1). This motivated us to undertake a more systematic study of the correlation between β and η using a standard model structure (LMoO(bdt); L = hydrotris(pyrazol-1-yl)borate). Here, we examine this relationship by systematically varying the fold angle of the model structure and calculating the theoretical SH parameters using DFT methodology.

The results highlight the potential shortcomings of predicting the Mo−dithilolate fold angle using in vacuo DFT optimization, especially where the energy barrier to a broad range of Mo−dithiolate fold angles is low. It is shown that a better estimate of the fold angle might be obtained by comparing the experimental and theoretical EPR parameters. In particular, we establish a relationship between the non-coincidence angle, β, and the metal−dithiolate fold angle, η, for the LMoO(bdt) model complex. Using this relationship, we show that experimental determination of β from EPR spectroscopy may provide a reliable measure of η. We suggest this represents a novel means of probing the electronic and geometric structure of the Mo^{V} intermediates in mononuclear Mo enzymes.

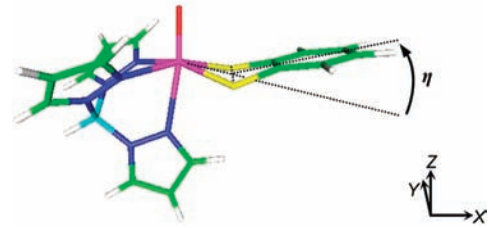

Figure 1. Schematic of the LMoO(bdt) model complex used in this study (Mo^{V} = violet, S = yellow, N = blue, C = green; B = aqua, H = white). The fold angle η was systematically varied over a range of 110°, incorporating both positive (depicted) and negative fold angles. The molecular axes *X* and *Z* define the $C_s^{(XZ)}$ mirror symmetry plane, where *Z* is directed along the Mo≡O bond.

Theoretical Calculations

Single-point calculations were carried out on an SGI Altix Bx2 supercomputer (64 Itanium 2 CPUs and 121 GB of total RAM) at the University of Queensland high-performance computing unit using the ORCA program.[19] As a starting point, we used the geometry-optimized structure of LMoO(bdt) obtained previously by Joshi et al.,[12] where the simplified ligand L was used in place of the full Tp* ligand (Tp* = hydrotris(3,5-dimethylpyrazol-1-yl)borate) by replacing the methyl groups of Tp* with hydrogen atoms. Following the approach of Domercq et al.,[20] the metal−dithiolate fold angle was then varied in ±10° increments by rotating the bdt ligand about an axis passing through the two S atoms while holding all remaining atoms fixed. Although a linear transit model[21] could also have been used, wherein the fold angle is held fixed while the remaining structure is geometry-optimized, the present approach was much simpler. The difference between the two approaches will be small for fold angles close to the lowest-energy structure, whereas for larger fold angles, the physical meaning of both methods will be equally limited.

The model structure has monoclinic ($C_s^{(XZ)}$) symmetry, with the molecular (*X*,*Y*,*Z*) axes defined such that *Z* is parallel to the Mo≡O bond and the *Y* axis is directed normal to the *XZ* mirror plane (Figure 1). Since the **g** and **A** interactions have only one principal axis in common, we used the (*x*,*y*,*z*) coordinate system to identify the principal directions of the **g** matrix and (*x*′,*y*′,*z*′) to identify those of the **A** matrix. Thus, g_{yy} and $A_{y'y'}$ are coaxial and normal to the Mo≡E (*E* = O, S) bond axis, and the non-coincidence angle β is a component of a general Euler rotation $R(\alpha,\beta,\gamma) = R_z(\gamma)\, R_y(\beta)$

(12) Joshi, H. K.; Cooney, J. J. A.; Inscore, F. E.; Gruhn, N. E.; Lichtenberger, D. L.; Enemark, J. H. *Proc. Natl. Acad. Sci. U. S. A.* **2003**, *100*, 3719–3724.
(13) Joshi, H. K.; Enemark, J. H. *J. Am. Chem. Soc.* **2004**, *126*, 11784–11875.
(14) Kirk, M. L.; McNaughton, R. L.; Helton, M. E. *Prog. Inorg. Chem.* **2004**, *52*, 111–212.
(15) Sproules, S. A.; Morgan, H. T.; Doonan, C. J.; White, J. M.; Young, C. G. *Dalton Trans.* **2005**, 3552–3557.
(16) Young, C. G. In *Comprehensive Coordination Chemistry II*; McCleverty, J. A., Meyer, T. J., Eds.; Elsevier Pergamon: Amsterdam, 2004; Vol. *4*, Chapter 4.7, sections 4.7.3.4.2.(ii) and 4.7.3.4.3, pp 415−527.
(17) Drew, S. C.; Young, C. G.; Hanson, G. R. *Inorg. Chem.* **2007**, *46*, 2388–2397.
(18) Drew, S. C.; Hill, J. P.; Lane, I.; Hanson, G. R.; Gable, R. W.; Young, C. G. *Inorg. Chem.* **2007**, *46*, 2373–2387.
(19) Neese, F. *ORCA*, version 2.4.26. ORCA is an ab initio, DFT and semiempirical electronic structure package. The latest stable ORCA version (currently 2.6.35) is available from http://www.thch.uni-bonn.de/tc/orca/.
(20) Domercq, B.; Coulon, C.; Fourmigué, M. *Inorg. Chem.* **2001**, *40*, 371–378.
(21) Himo, F. *Theor. Chem. Acc.* **2006**, *116*, 232–240.

$R_z(\alpha)$ transforming the principal axes of **g** to those of **A**.

As used previously,[17] the coupled-perturbed self-consistent field (CP-SCF) formalism implemented in the ORCA program was applied to calculate both the **g** and the ^{95}Mo **A** matrices at one consistent level of theory. Briefly, the hyperfine matrix **A** was obtained from the sum of the isotropic Fermi contact contribution (A_F), the traceless first-order anisotropic spin-dipolar contribution ($\mathbf{A}^{dip}$), and the nontraceless second-order contribution ($\mathbf{A}^{SO}$), which incorporates spin−orbit coupling (SOC) of excited states into the SOMO:[22−24]

$$A_{\mu\nu} = \delta_{\mu\nu}A_F + A_{\mu\nu}^{dip} + A_{\mu\nu}^{SO} \quad (1)$$

The **g** matrix was obtained from the sum of the second-order cross-terms between the orbital Zeeman (OZ) and SOC operators, a relativistic mass correction (RMC), and a diamagnetic gauge correction (GC): [25]

$$g_{\mu\nu} = \delta_{\mu\nu}g_e + \Delta g_{\mu\nu}^{RMC} + \Delta g_{\mu\nu}^{GC} + \Delta g_{\mu\nu}^{OZ/SOC} \quad (2)$$

where $g_e = 2.0023$ is the free electron g value. The spin-unrestricted Kohn−Sham equations were solved self-consistently and tightly converged using (i) the BP86 GGA functional incorporating Becke 88 exchange[26] and the Perdew 86 correlation[27] and (ii) the B3LYP hybrid functional incorporating Becke 88 exchange and Lee−Yang−Parr gradient-corrected correlation[28] and the three empirical parameters of Becke.[29] Scalar relativistic effects were treated at the all-electron level using the zeroth-order regular approximation[30] using the model potential implementation of van Wüllen,[31] in conjunction with a polarized triple-ζ (TZVP) basis for Mo;[32] a TZVP basis for all N, S, and O atoms;[33] and an SV(P) basis[34] on all C, H, and B atoms. The BP86 calculations employed the split-RI-J Coulomb approximation implemented in ORCA[19] using a suitable TZV auxiliary basis.[35] To add flexibility to the core of the Mo atom, all bases were fully decontracted and the integration accuracy increased,[36] which ensured an accurate electron density at the Mo nucleus and hence a sensible prediction of the isotropic ^{95}Mo hyperfine coupling. An accurate mean-field method was used to account for the one- and two-electron (spin-own-orbit and spin-other-orbit) contributions to the Breit−Pauli spin−orbit coupling operator.[37] Using this effective SOC operator, the **g** and the ^{95}Mo **A** matrices were computed using the CP-SCF formalism.[38−41]

The non-coincidence between the principal **g** and **A** coordinate systems was specified by three Euler rotations, $R(\alpha,\beta,\gamma) = R_z(\gamma)\,R_y(\beta)\,R_z(\alpha)$, that transform the principal **g** coordinate system into the principal **A** coordinate system, consisting of three consecutive rotations, α, β, and γ, about the z, the (new) y, and the (new) z axes, respectively. Here, a positive rotation angle was defined to correspond to an anticlockwise rotation, looking toward the origin. Additional details are provided in the Supporting Information.

In order to analyze the character of the MOs in terms of a more intuitive ligand field picture, we used the method of quasi-restricted molecular orbitals (QROs)[19,42] implemented in the ORCA program, as described in our previous study.[17] The QRO picture enables one to compensate for the fact that the spin-polarized canonical molecular orbitals formed from the unrestricted Kohn−Sham determinant possess appreciably different spatial and energetic behavior. It must be borne in mind, however, that, while the spin Hamiltonian parameters were computed at the B3LYP level, the QRO analysis can only be implemented at the BP86 level. In the latter instance, Δ**g** and **A** are both underestimated compared with the hybrid B3LYP calculations[17] due to the well-known tendency for pure functionals to overestimate the covalency of polar metal−ligand bonds.[24] Nevertheless, the QRO analysis enables a qualitative description of the electronic structure that is responsible for the spin Hamiltonian parameters obtained from the more complicated CP-SCF calculation. The QROs were rendered for display using gOpenMol.[43]

Starting from the geometry-optimized structure of Enemark and co-workers,[12] the above methodology was used to compute the SH parameters over a range of metal−dithiolate fold angles by manually bending the bidentate bdt ligand in 10° increments about an axis bisecting the equatorial sulfur atoms, while holding all other bond angles and lengths constant (Figure 1). We chose to start from a geometry-optimized structure rather than that available from X-ray crystallography, since the former possesses ideal C_s symmetry, which can be maintained over a wide range of fold angles.

A note on the convention used for assigning the principal axes of **g** and **A** is in order. In our earlier studies, we chose to assign the smallest g value and largest A value to the principal z and z' axes of the symmetric $\mathbf{g}.\mathbf{g}^T$ and $\mathbf{A}.\mathbf{A}^T$ matrices, respectively. This arbitrary assignment was made since this led to non-coincidence angles $\beta < 45°$. In the present study, we found it more intuitive to instead assign the largest g value to the principal z axis of $\mathbf{g}.\mathbf{g}^T$, since this resulted in most non-coincidence angles falling in the range $-45 < \beta < 45°$ for the LMoO(bdt) complex over the range of fold angles examined. A detailed derivation of the relationship between the Euler angles associated with these and other conventions used in the literature is provided as Supporting Information.

(22) Keijzers, C. P.; de Boer, E. *J. Chem. Phys.* **1972**, *57*, 1277–1281.
(23) Belanzoni, P.; Baerends, E. J.; van Asselt, S.; Langewen, P. B. *J. Phys. Chem.* **1995**, *99*, 13094–13102.
(24) Neese, F. *J. Phys. Chem. A* **2001**, *105*, 4290–4299.
(25) Kaupp, M.; Bühl, M.; Malkin, V. G.; *Calculation of NMR and EPR Parameters, Theory and Applications*; Wiley-VCH, Weinheim, Germany, 2004.
(26) Becke, A. D. *Phys. Rev. A: At., Mol., Opt. Phys.* **1988**, *38*, 3098–3100.
(27) Perdew, J. P. *Phys. Rev. B: Condens. Matter Mater. Phys.* **1986**, *33*, 8822–8824.
(28) Lee, C.; Yang, W.; Parr, R. G. *Phys. Rev. B: Condens. Matter Mater. Phys.* **1988**, *37*, 785–789.
(29) Becke, A. D. *J. Chem. Phys.* **1993**, *98*, 5648–5652.
(30) (a) van Lenthe, E.; Baerends, E. J.; Snijders, J. G. *J. Chem. Phys.* **1993**, *99*, 4597–4610. (b) van Lenthe, E.; Baerends, E. J.; Snijders, J. G. *J. Chem. Phys.* **1996**, *105*, 6505–6516. (c) van Lenthe, E.; van der Avoird, A.; Wormer, P. E. S. *J. Chem. Phys.* **1998**, *108*, 4783–4796.
(31) van Wüllen, C. *J. Chem. Phys.* **1998**, *109*, 392–399.
(32) Ahlrichs, R.; May, K. *Phys. Chem. Chem. Phys.* **2000**, *2*, 943–945.
(33) Schäfer, A.; Horn, H.; Ahlrichs, R. *J. Chem. Phys.* **1992**, *97*, 2571–2577.
(34) Schäfer, A.; Huber, C.; Ahlrichs, R. *J. Chem. Phys.* **1994**, *100*, 5829–5835.
(35) (a) Eichkorn, K.; Treutler, O.; Ohm, H.; Haser, M.; Ahlrichs, R. *Chem. Phys. Lett.* **1995**, *240*, 283–289. (b) Eichkorn, K.; Weigend, F.; Treutler, O.; Ahlrichs, R. *Theor. Chem. Acc.* **1997**, *97*, 119−124. The Mo atom used an uncontracted basis constructed "by inspection" in the ORCA program.
(36) The SpecialGridIntAcc parameter in ORCA was set to 14, 7, 5, and 5 for Mo, S, N, and O atoms, respectively.
(37) Neese, F. *J. Chem. Phys.* **2005**, *122*, 034107/1−13.
(38) Neese, F. *J. Chem. Phys.* **2001**, *115*, 11080–11096.
(39) Neese, F. *J. Chem. Phys.* **2003**, *118*, 3939–3948.
(40) Baute, D.; Arieli, D.; Neese, F.; Zimmermann, H.; Weckhuysen, B. M.; Goldfarb, D. T. *J. Am. Chem. Soc.* **2004**, *126*, 11733−11745.
(41) Jensen, F. *Introduction to Computational Chemistry*; John Wiley and Sons: Chichester, U. K., 2002.
(42) Schöneboom, J C.; Neese, F.; Thiel, W. *J. Am. Chem. Soc.* **2005**, *127*, 5840−5853.
(43) gOpenMol for Windows, v. 3.00, 2005. http://www.csc.fi/gopenmol/UT (accessed Jan 2009).

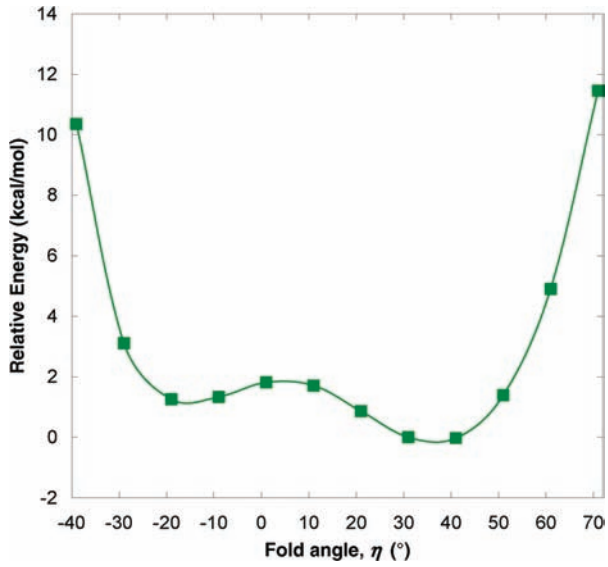

Figure 2. Total energy of the model LMoO(bdt) structure as a function of the metal−dithiolate fold angle. Starting from the in vacuo geometry-optimized structure of ref 13 ($\eta = 31°$), the fold angle was systematically varied while holding the remaining bond angles and lengths fixed (Figure 1).

Results and Discussion

A Low-Energy Barrier to a Wide Range of Mo−Dithiolate Fold Angles. An energy scan as a function of fold angle (Figure 2) revealed a double-well potential with a barrier height of only ∼2−3 kcal/mol. Similar behavior has been found for other open-shell d^1 Mo−dithiolate complexes, where a very low energy barrier (<1 kcal mol^{-1}) separating positive and negative fold angles was identified for the complexes $Cp_2Mo(dmit)^{\bullet+}$ and $Cp_2W(dmit)^{\bullet+}$ (Cp = cyclopentadienyl; $dmit^{2-}$ = 2-thioxo-1,3-dithiole-4,5-dithiolate).[20] A global energy minimum between $\eta = 30°$ and 40° can be identified, in general agreement with Joshi et al.,[12] whose geometry-optimized structure had a fold angle of 31.0°,[44] and the positive fold angle of 21.3° adopted by Tp*MoO(bdt) in the solid state.[45] Another local energy minimum could also be identified at a fold angle near −20°, which lies on the other side of the double well. Importantly, Figure 2 indicates that a range of positive fold angles can be adopted at a very low energy cost.

Dependence of g and A Principal Axes on the Fold Angle. For each fold angle, the **g** and **A** matrices were calculated at the B3LYP level using the CP-SCF formalism. Their principal components are listed in Table 1 and plotted graphically in Figures S2−S3 (Supporting Information), while Figure 3 displays the angular dependence of the principal **g** and **A** directions, together with their relative orientation (defined by the Euler angle β). It is evident that the maximum non-coincidence angle is not predicted to exceed 60° and that the greatest sensitivity of β to changing fold angle is in the region $\eta = [-20, 20]°$, where $d\beta/d\eta$ is the largest.

Our earlier experimental EPR and theoretical DFT study of a set of different, but related, complexes showed that the principal directions of the **A** and **g** axes of molybdenyl and thiomolybdenyl complexes could be correlated with the configurational mixing of the metal-centered SOMO and lowest unoccupied molecular orbital (LUMO).[17,18] In particular, we proposed a tractable relationship between the metal−di(thi)olate fold angle of Tp*MoEX (E = O,S; X = cat, bdt; cat = catecholate) complexes and the noncoincidence angle β defining the relative orientation of **g** and **A**. However, the different chemical composition of each complex made it difficult to establish a general trend. To further examine the relationship between the principal directions of **g** and **A** and the fold angle η, we analyzed the Löwdin reduced orbital populations of the QROs over a wide range of fold angles for the LMoO(bdt) model complex to determine the electronic origin of the fold-angle dependence of **g** and **A**.

The orientation of **A** (relative to the molecular coordinate frame) correlates with the admixture of d_{XZ} into the $d_{X^2-Y^2}$-based SOMO (Figure 5), which is associated with a rotation of the plane of the SOMO (Figure 4).[17] We previously ascribed the substantial rotation of the principal **g** axes in the $C_S^{(XZ)}$ mirror plane to an admixture of d_{XY} character into the d_{YZ}-based antibonding LUMO.[17,18] To investigate this in more detail, we examined the contribution of the SOMO → LUMO d−d transition to Δg_{XZ}, the latter of which is only nonzero when the principal directions of **g** deviate from the molecular *X* and *Z* directions (Figure 1). The analysis in Figure 6 shows that, when η is large and positive, the spin−orbit coupling of the SOMO to the LUMO accounts for the majority of Δg_{XZ}. In comparison, the DOMO → SOMO transitions (DOMO = doubly occupied molecular orbital), which include ligand-to-metal charge transfer (LMCT) transitions, make a modest net (positive) contribution, as do the remaining SOMO → VMO transitions (VMO = virtual molecular orbital).[46] A simple crystal field theory description of the electronic structure of a d^1 system in $C_s^{(XZ)}$ symmetry predicts that both an admixture of d_{XZ} character into the $d_{X^2-Y^2}$-based SOMO ($d_{X^2-Y^2}$ and d_{XZ} transform as A′) and an admixture of d_{XY} character into the d_{YZ}-based LUMO (d_{XY} and d_{YZ} transform as A″) can generate off-diagonal matrix elements g_{XZ} and hence effect a rotation of the principal axes of **g** about the molecular *Y* axis.[47] Figure 7 compares these admixtures for LMoO(bdt) and correlates them with Δg_{XZ} as a function of the fold angle. It is evident that the magnitude and sign of Δg_{XZ} correlates strongly with the d_{XZ} admixture in the SOMO, whereas the d_{XY} admixture in the LUMO varies only modestly as a function of η. This behavior is also apparent from Figure 4, where the plane of the metal-centered lobes of the LUMO appears effectively constant, whereas the metal-centered lobes of the SOMO visibly rotate

(44) The precise energy minimum may differ in the present instance, due to the inclusion of relativistic terms at the all-electron level instead of using effective core potentials.
(45) Dhawan, I. K.; Enemark, J. H. *Inorg. Chem.* **1996**, *35*, 4873–4882.
(46) The magnitude of any of the individual DOMO → SOMO and SOMO → VMO transitions is also small (data not shown).
(47) Young, C. G.; Enemark, J. H.; Collison, D.; Mabbs, F. E. *Inorg. Chem.* **1987**, *26*, 2925–2927.

Table 1. Theoretical **g** and **A**(^{95}Mo) Parameters for LMoO(bdt) Model Complex As a Function of Metal−Dithiolate Fold Angle[a,b]

η (deg)	g_{xx}	g_{yy}	g_{zz}	g_{iso}	$A_{x'x'}$ (^{95}Mo)	$A_{y'y'}$ (^{95}Mo)	$A_{z'z'}$ (^{95}Mo)	A_{iso} (^{95}Mo)	α^c	β^c	γ^c
−39	1.9439	1.9731	2.0093	1.9754	17.83	14.86	43.81	25.52	0.3	−26.7	−0.7
−29	1.9496	1.9802	2.0120	1.9806	16.86	12.18	41.85	23.65	0.5	−24.5	−0.5
−19	1.9551	1.9860	2.0127	1.9843	15.64	9.38	40.34	21.80	0.4	−17.9	−0.1
−9	1.9578	1.9868	2.0105	1.9851	14.72	7.39	40.70	20.95	−2.3	−4.7	2.9
1	1.9528	1.9844	2.0075	1.9816	14.97	8.03	44.40	22.48	2.4	16.5	−1.7
11	1.9411	1.9794	2.0095	1.9767	16.43	12.00	49.41	25.96	1.3	36.1	−0.7
21	1.9310	1.9745	2.0154	1.9736	17.79	16.91	52.21	28.99	0.9	48.0	−0.2
31[d]	1.9242	1.9691	2.0189	1.9707	18.04	20.24	52.46	30.27	0.8	53.2	−0.2
41	1.9186	1.9622	2.0191	1.9666	17.34	21.79	51.64	30.28	0.8	56.9	−0.2
51	1.9138	1.9532	2.0176	1.9615	16.25	22.26	50.56	29.71	0.8	57.8	−0.5
61	1.9107	1.9421	2.0152	1.9560	15.41	22.32	49.59	29.13	0.8	57.7	−0.3
71	1.9112	1.9289	2.0124	1.9508	15.58	22.48	48.98	29.03	0.3	56.6	−0.4

[a] Experimental data are provided in Table 2. [b] Hyperfine data is expressed in units of 10^{-4} cm^{-1}. [c] Euler rotations (in degrees) are defined as $R(\alpha,\beta,\gamma) = R_z(\gamma)\ R_y(\beta)\ R_z(\alpha)$. [d] Geometry-optimized structure determined in ref 12.

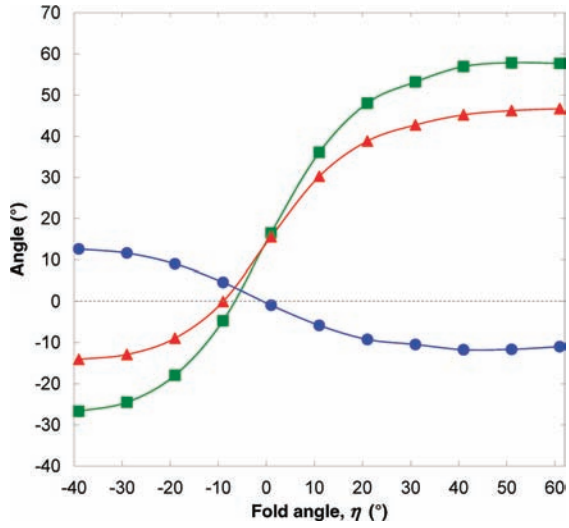

Figure 3. Fold angle dependence of the angle $\angle zZ$ between the Mo≡O (Z) direction and the principal g_{zz} direction (▲), the angle between Z and the principal $A_{z'z'}$ direction (●), and the net non-coincidence β between principal g_{zz} and $A_{z'z'}$ directions (■). The angle β represents the Euler rotation $R(\alpha,\beta,\gamma) = R(0,\beta,0)$ that transforms the principal coordinate system of **g** into that of **A**. The data was obtained from CP-SCF calculations at the B3LYP level.

as η varies. The reason for this may be the antibonding nature of the Mo≡O bond, which could restrict the degree to which the metal-centered orbital lobes can vary their orientation.

Interestingly, when the complex is completely unfolded ($\eta = 0°$), the SOMO is essentially pure $d_{x^2-y^2}$, **A** is coincident with the molecular symmetry axes defined in Figure 1, and the non-coincidence angle β is equivalent to $\angle zZ$. Moreover, in the vicinity of $\eta = -10°$, configurational mixing in both the SOMO and LUMO is low and the non-coincidence angle β approaches 0°. This leads to orthorhombic spin Hamiltonian parameters even though the point symmetry is only monoclinic and highlights the important role η plays in determining the electronic structure.

Geometry-Optimization in vacuo as a Predictor of the Experimental Fold Angle. Although the structure adopted in frozen solution is not known a priori and may not be accurately reflected by either crystallographic or geometry-optimized structures, our earlier DFT study of the bidentate Tp*MoEX (E = O,S) series of complexes suggested that the crystallographic structure of Tp*MoO(bdt) provided a more realistic representation of the true solution than the in vacuo DFT-optimized structure. In particular, the former led to a theoretically predicted value of β within 1° of that determined from frozen solution EPR data (Table 2).[17]

Given the above discrepancy between the crystallographic and in vacuo optimized structures, it is interesting to ask whether the theoretical SH parameters derived from the crystal structure could be made to correlate with those from the in vacuo structure if the latter was bent to the same fold angle. A comparison of the theoretical parameters obtained from the crystallographic structure of Tp*MoO(bdt) with those derived from the fold angle study of LMoO(bdt) shows that the best overall correlation does indeed occur near a fold angle of 20°, in good agreement with the crystallographic 21.3° fold angle (Table 2). In particular, bending the geometry-optimized structure of LMoO(bdt) to a fold angle of 21° yields a theoretical Euler angle of $\beta = 48°$ (Figure 3, Table 1.), which compares with $\beta = 44°$ when the actual crystallographic structure of Tp*MoO(bdt) is used,[17] and with $\beta = 45°$ obtained from experimental EPR of Tp*MoO(bdt) in frozen solution.[18] The bent geometry at $\eta = 21°$ also appears to improve the agreement of the theoretical principal g values with experimental results, compared with the theoretical g values obtained using the X-ray crystallographic structure (Table 2).

Experimental SH Parameters as Predictors of the Metal−Dithiolate Fold Angle. The above observations suggest that, even when the gross geometric structure may not be precisely known, the non-coincidence of **g** and **A** may still remain a useful indicator of the metal−dithiolate fold angle. Thus, given a set of low-symmetry experimental EPR data, we may use our model data to infer the metal−dithiolate angle of the Mo^V center in the absence of a crystallographic structure. When Figure 3 is used, the experimentally determined Euler angle of $\beta = 45°$ for Tp*MoO(bdt) (Table 1) may be associated with a fold angle of $\eta = 18°$, which is close to the $\eta = 21.3°$ determined from X-ray crystallography.

The present theoretical data also appear useful in predicting the fold angle of the sulfido analogue compound Tp*MoS(bdt). The experimental Euler angle determined from frozen solution EPR was $\beta = 39°$[18] ($\beta = 51°$ using the convention in this work; see the Supporting Information). When Figure 3 is used, $\beta = 51°$ is associated with a fold angle of $\eta \approx 25°$, which agrees well with the metal−dithiolate

Table 2. Experimental and Theoretical EPR Parameters of Mo^V from Tp*MoO(bdt) and Tp*MoS(bdt)[a]

system	g_{xx}	g_{yy}	g_{zz}	g_{iso}	$A_{x'x'}$ (^{95}Mo)[b]	$A_{y'y'}$ (^{95}Mo)[b]	$A_{z'z'}$ (^{95}Mo)[b]	A_{iso} (^{95}Mo)	α^c	β^c	γ^c	η^d
Tp*MoO(bdt) Exp[e]	1.9360	1.9730	2.0025	1.9705	24.00	26.00	60.00	36.70	0	45	0	18
LMoO(bdt) DFT (bent structure at $\eta = 18°$)[f]	1.933	1.975	2.014	1.974	17.4	15.4	51.5	28.1	1	45	0	18
Tp*MoO(bdt) DFT (crystallographic structure)[g,h]	1.9508	1.9863	2.0161	1.9771	18.90	18.10	52.60	29.90	1	44	−1	17
LMoO(bdt) DFT (bent structure at $\eta = 21°$)[i]	1.9310	1.9745	2.0154	1.9736	17.79	16.91	52.21	28.99	1	48	0	21
Tp*MoS(bdt) Exp[e]	1.9159	1.9680	1.9975	1.9605	26.0	26.5	59.2	37.2	0	51	0	25
Tp*MoS(bdt) DFT (crystallographic structure)[h,j]	1.9643	1.9756	2.0009	1.9643	22.0	22.5	54.9	33.1	−1	52	3	27

[a] A prediction for the metal−dithiolate fold angle is provided by comparing the LMoO(bdt) model data from Figure 3 with the experimentally-determined non-coincidence angle β. [b] Hyperfine data are expressed in units of 10^{-4} cm^{-1}. [c] Euler rotations (in degrees) are defined as $R(\alpha,\beta,\gamma) = R_z(\gamma)\, R_y(\beta)\, R_z(\alpha)$. [d] Predicted fold angle obtained by comparing β with the LMoE(bdt) (E = O, S) model data in Figure 3. [e] Experimental parameters obtained from frozen solution EPR; ref 18. [f] Theoretical parameters obtained from DFT by extrapolating the data of Figures 3, S2, and S3 at $\eta = 18°$. [g] Theoretical parameters computed from DFT using the X-ray crystallographic structure ($\eta = 21.3°$); ref 17. [h] Corrections to Euler angles published in ref 17 appear in the Supporting Information. [i] Theoretical parameters obtained from DFT by extrapolating the data of Figures 3, S2, and S3 at $\eta = 21°$. [j] Theoretical parameters computed from DFT using the X-ray crystallographic structure ($\eta = 25.3°$); ref 17.

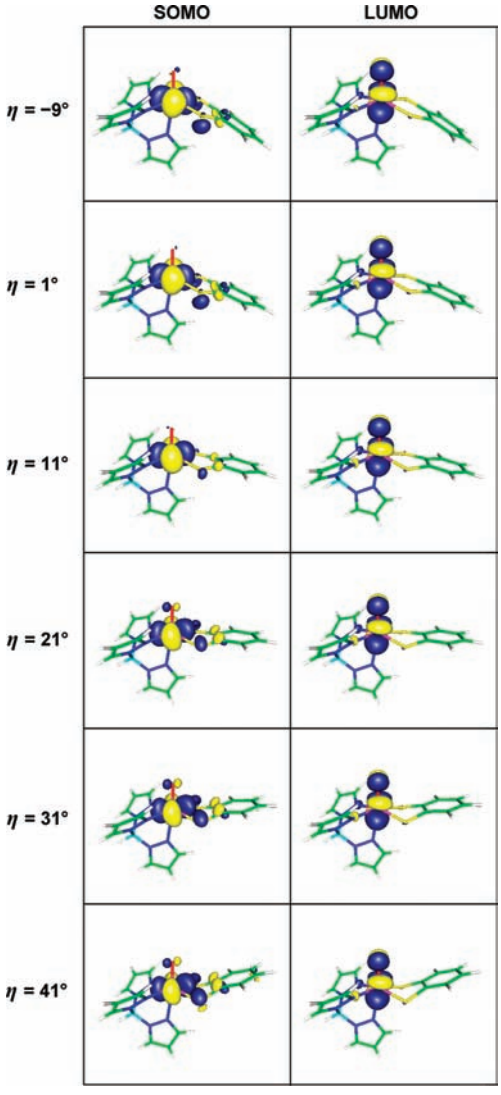

Figure 4. Quasi-restricted molecular orbitals corresponding to the SOMO and LUMO, for a selected range of fold angles. Note the counterclockwise rotation of the lobes of the SOMO about the molecular *Y* axis (directed into the page) as η increases. Contours are drawn at ±0.05.

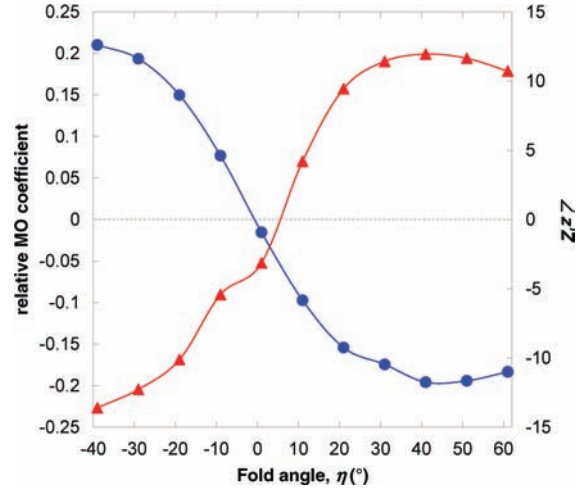

Figure 5. Correlation of the principal $A_{z'z'}$ direction with configurational mixing within the SOMO as a function of fold angle. An admixture of d_{xz} into the $d_{x^2-y^2}$-based SOMO (▲) results in a rotation of the positive lobes of the $d_{x^2-y^2}$-based orbital, with a concomitant rotation of the principal $A_{z'z'}$ direction away from the molecular *Z* (Mo≡O bond) axis by an angle $\angle z'Z$ (●). The rotation $\angle z'Z$ was determined at the B3LYP level. The MO coefficients pertaining to the character of the SOMO were determined at the BP86 level from the square roots of the respective Löwdin reduced orbital populations of the singly occupied quasi-restricted molecular orbital. The ratio of the d_{xz} and $d_{x^2-y^2}$ coefficients was plotted (▲), with the sign being determined by visual inspection of the geometric nature of the SOMO (Figure 4).

fold angle of 25.3° determined from X-ray crystallography.[18] The crystallographic data indicate that both Tp*MoO(bdt) and Tp*MoS(bdt) possess the same E≡Mo−S and Mo−S−C bond angles, and it is only the MoS_2C_2 fold angle that differs.[18] The ability to apply our model to a thiomolybdenyl analogue rests with the observation that, although the weaker π-donor terminal sulfido ligand yields a smaller SOMO−LUMO gap and increased *g* shifts compared with its oxo counterpart, this increase applies not only to Δg_{XX} and Δg_{ZZ} but also to the off-diagonal Δg_{XZ} element. Hence, the orientation of **g**, which is directly related to Δg_{XZ} (Figure 6), is not dramatically affected upon substituting Mo^V≡O with Mo^V≡S. Likewise, the orientation of **A** is determined primarily by the orientation of the plane of the SOMO (Figure 5), which is not greatly affected by a change from an apical oxo to sulfido liagnd.[17] Hence, the non-coincidence angle of **g** and **A** can still be determined with confidence.

It must be stressed that, in applying our model, the geometry used did not correspond to the global energy minimum predicted in vacuo; that is, we have forced the system into a higher energy state in order to model the effects of other structural factors for which the simple LMoO(bdt) complex cannot account. As observed by Domercq et al.,[20] a low-energy barrier to changing the fold angle endows the Mo−dithiolate system with a versatile and highly flexible

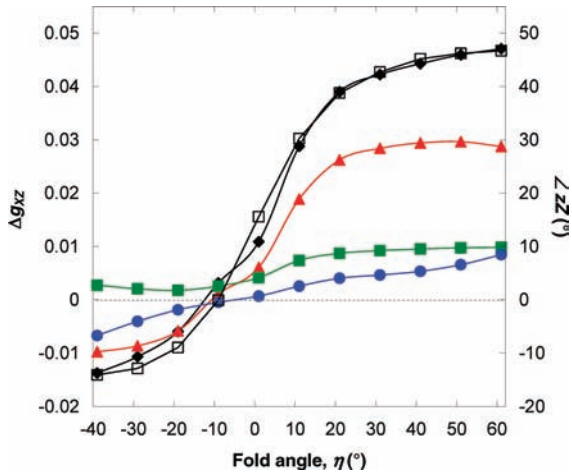

Figure 6. Relative contribution of the SOMO → LUMO d−d transition (▲) to the Δg_{XZ} component (◆) of the g shift matrix $\Delta g_{ij} = g_{ij} - \delta_{ij}g_e$, which effects a rotation $\angle zZ$ (□) of the principal g_{zz} direction away from the molecular Z axis. The net contribution from all DOMO → SOMO transitions (■) and all SOMO → VMO transitions other than SOMO → LUMO (●) contribute a relatively small amount to Δg_{XZ} in the vicinity of the experimentally observed positive fold angles. The QRO analysis at the BP86 level took into account ±40 QROs above/below the SOMO.

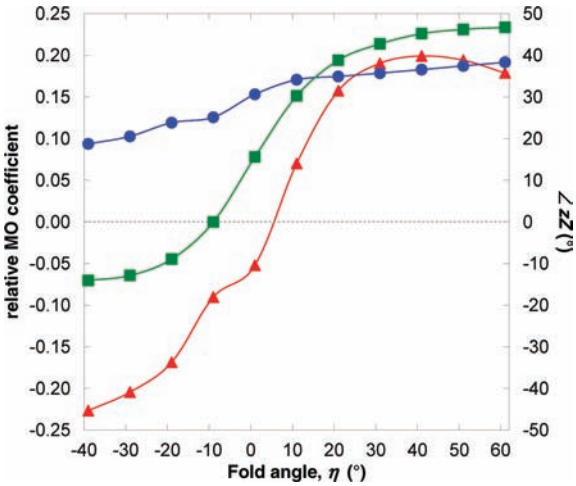

Figure 7. Correlation of the principal g_{zz} direction (■) with the admixture of d_{XZ} into the SOMO (▲) and of d_{XY} into the LUMO (●). The large SOMO → LUMO contribution to Δg_{XZ} clearly requires configurational mixing in both orbitals to effect a rotation of the **g** matrix. The MO coefficients pertaining to the d_{XZ} and $d_{X^2-Y^2}$ character of the SOMO and the d_{XY} and d_{YZ} character of the LUMO were determined at the BP86 level from the square roots of the respective Löwdin reduced orbital populations of the singly occupied QRO and lowest unoccupied QRO. The ratios of the d_{XZ} and $d_{X^2-Y^2}$ coefficients (▲) and of the d_{XY} and d_{YZ} coefficients (●) were determined, with the sign being determined by visual inspection of the geometric nature of the SOMO and LUMO, respectively (Figure 4).

molecular structure. In their studies of Cp_2Mo(dithiolene) salts in an [AsF_6^-] crystal host, they found that the molecular structure adopted by the organometallic complexes was largely correlated with the nature, shape, and symmetry of the counteranions of the host crystal. In this way, different crystal structures could be correlated with different fold angles, thereby altering intermolecular interactions between the organometallic units and leading to different solid-state magnetic properties.[20] We may postulate that a similar effect operates for the LMoO(bdt) complex, in addition to the enzyme active sites upon which it is based, whereby the fold angle adopted in nature will depend critically upon the identity of physiological counterions as well as coligands trans to the dithiolate moiety, thereby altering electron transfer interactions with redox partners.

With this in mind, our study of the LMoO(bdt) model complex indicates that, over a limited range of fold angles to which the energy barrier is low (Figure 1), the treatment has some predictive power by enabling a measure of the fold angle from the randomly oriented EPR spectrum. This raises the possibility that experimental EPR data could also be used to probe the metal−dithiolate fold angle of Mo^V intermediates in enzymes.

Comparison with Mononuclear Mo Enzymes. Joshi and Enemark[13] have exploited the availability of a high-resolution crystal structure for aldehyde oxidase (AO), a member of the xanthine oxidase (XO) family, to study changes in the Mo−MPT fold angle as a function of the oxidation state of the active site. Here, the X-ray crystal structure[48] provided an input geometry for in vacuo DFT optimization of the oxidized and reduced active site, which predicted a fold angle decrease from 42.6° in the fully oxidized aqua complex (12.3° for the hydroxo form, which is believed to better reflect the crystal structure) to 10.4° upon reduction to the Mo^{IV} oxidation state. The crystal structure of the oxidized active site possesses a fold angle of 16.6°.[13] Assuming that the fold angle of the Mo^V intermediate will fall somewhere between the Mo^{VI} (η = 16.6°) and Mo^{IV} (η = 10.4°) geometries, we can use our LMoO(bdt) model to predict a sizable non-coincidence angle of $\beta \sim 35-45°$ for the Mo^V intermediate of AO. It would be useful to compare these angles with experimental EPR spectroscopic parameters, but unfortunately no spectral data relating the principal **g** and **A**(^{95}Mo) principal directions appear currently available for this enzyme.

Experimentally determined non-coincidence angles are available, on the other hand, for the "very rapid" signal of XO,[49] in addition to the low and high pH forms of sulfite oxidase (SO)[50] (Table 3). While there is a strong degree of variability in the crystallographic data depending upon which a substrate or inhibitor is present, most crystal structures of xanthine dehydrogenase (XDH) and its proteolytic cleavage product xanthine oxidase (XO) (EC: 1.17.1.4, 1.17.3.2, 1.1.1.204, 1.1.3.22, 1.2.1.37,1 0.2.3.2) indicate a fold angle ≥ 20°.[51] When our LMoO(bdt) data is used as a model, the experimental non-coincidence of β = 36° is predicted to be associated with a fold angle of $\eta \approx 11°$ for the very rapid Mo^V intermediate of XO (Figure 3). In the case of the low pH form of SO, a fold angle of $\eta \approx 2°$ is predicted from the observed non-coincidence of β = 18°. Crystallographic data

(48) Rebelo, J. M.; Dias, J. M.; Huber, R.; Moura, J. J. G.; Romao, M. J. *J. Biol. Inorg. Chem.* **2001**, *6*, 791–800.
(49) George, G. N.; Bray, R. C. *Biochemistry* **1988**, *27*, 3603–3609.
(50) Dhawan, I. K.; Enemark, J. H. *Inorg. Chem.* **1996**, *35*, 4873–4882.
(51) (a) Enroth, C.; Eger, B. T.; Okamoto, K.; Nishinoi, T.; Nishino, T.; Pai, E. F. *Proc. Natl. Acad. Sci. U. S. A.* **2000**, *97*, 10723–10728. (b) Okamoto, K.; Eger, B. T.; Nishino, T.; Kondo, S.; Pai, E. F.; Nishino, T. *J. Biol. Chem.* **2003**, *278*, 1848–1855. (c) Okamoto, K.; Matsumoto, K.; Hille, R.; Eger, B. T.; Pai, E. F.; Nishino, T. *Proc. Nat. Acad. Sci. U. S. A.* **2004**, *101*, 7931–7936. (d) Fukunari, A.; Okamoto, K.; Nishino, T.; Eger, B. T.; Pai, E. F.; Kamezawa, M.; Yamada, I.; Kato, N. *J. Pharm. Exp. Ther.* **2004**, *311*, 519–528. (e) Pauff, J. M.; Zhang, J.; Bell, C. E.; Hille, R. *J. Biol. Chem.* **2008**, *283*, 4818–4824.

Table 3. Experimental EPR Parameters of Mo^V Species in Various Molybdenum Enzymes[a]

system	g_{xx}	g_{yy}	g_{zz}	g_{iso}	$A_{x'x'}(^{95}Mo)$[b]	$A_{y'y'}(^{95}Mo)$[b]	$A_{z'z'}(^{95}Mo)$[b]	$A_{iso}(^{95}Mo)$	α[c]	β[c]	γ[c]	η[d]
SO (low pH form)[e,f]	1.968	1.974	2.007	1.983	16.7	25.0	56.7	32.8	0	18	0	2
SO (high pH form)[e,f]	1.954	1.966	1.990	1.970	11.3	21.0	54.4	28.9	59	26	−56	5
XO (rapid type 1, formamide)[g]	1.9666	1.9710	1.9901	1.9759	25.7	24.7	61.4	37.4	0	18	0	2
XO (rapid type 1, 1-methylxanthine)[h]	1.9646	1.9691	1.9886	1.9741	24.8	24.8	61.7	37.1	0	20	0	3
XO (very rapid, xanthine)[g]	1.9494	1.9550	2.0252	1.9765	19.1	18.2	44.4	27.2	8	36	0	11
XO (very rapid, 2-oxo-6-methylpurine)[g]	1.9446	1.9518	2.0229	1.9731	21.2	20.0	42.2	29.5	7	42	0	15

[a] A prediction for the metal−dithiolate fold angle is provided by comparing the model data from Figure 3 with the experimentally-determined non-coincidence angle β. [b] Hyperfine data are expressed in units of 10^{-4} cm^{-1}. [c] Euler rotations (in degrees) are defined as $R(\alpha,\beta,\gamma) = R_z(\gamma)\, R_y(\beta)\, R_z(\alpha)$. [d] Predicted fold angle obtained by comparing β with the LMoO(bdt) model data in Figure 3. [e] Spin Hamiltonian parameters have been redefined with respect to the original reference such that g_{zz} and $A_{z'z'}$ are the largest principal values (see the Supporting Information). [f] Experimental EPR data obtained from ref 50. [g] Experimental EPR data obtained from ref 49. [h] Experimental EPR data obtained from ref 54.

for SO reveal a fold angle in the vicinity of 8−11°.[52] At best, the crystallographic structures represent a weighted mean of the oxidation state (VI, V, and IV) of the Mo ion as radiation damage from intense synchrotron sources is well-known to reduce metal ions. Consequently, it is difficult to assess the accuracy of the present predictions for the Mo^V intermediates. Moreover, there are other major structural differences between the model complex and real enzymes which may be more important than just the metal−dithiolate fold angle (e.g., the angle between the terminal oxo, Mo, and the bisector of the sulfur atoms is around 105° for LMoO(bdt) but 115−130° in XO and XDH crystal structures[51]). Nevertheless, the fold angles predicted by our Mo^V model system are smaller than those observed in the nominally Mo^{VI} state, consistent with the above DFT studies of the AO model structure where a decrease in fold angle was predicted to occur during Mo reduction.[13] Similar behavior has been observed in studies of Cp_2Mo(dithiolene) complexes (Cp = cyclopentadiene), where the decrease in fold angle from around 30° in the Mo^V state to 0° in the Mo^{IV} state[20] was attributed to the overlap stabilization of the empty metallic and occupied dithiolene frontier orbitals in the folded conformation.[20,53]

Clearly the point symmetry at the active site of all Mo enzymes will be triclinic rather than the idealized $C_s^{(XZ)}$ symmetry of the LMoO(bdt) model complex. In some instances, experimental EPR data of Mo^V enzyme intermediates have been simulated using monoclinic symmetry ($\alpha = \gamma = 0$), whereas the simulated parameters for the very rapid XO species ($\alpha = 7-8°$) and the high pH form of SO ($\alpha = 59°$, $\beta = 26°$, $\gamma = -56°$) are triclinic (Table 3). In the case of the former, one can argue that $\alpha = 7-8°$ represents a small deviation from ideal $C_s^{(XZ)}$ symmetry, such that a prediction of the fold angle using the model complex data is still valid. However, the latter represents a more significant deviation from monoclinic symmetry; therefore, although we provide a predicted value of η based upon the model complex data (Table 3), it is unclear whether such a comparison is meaningful. From our earlier DFT studies of triclinic Tp*$MoEX_2$ compounds (E = O, S; X = 2-(ethylthio)phenolate, 2-(*n*-propyl)phenolate), a nonzero value of α was associated with a rotation of the LUMO and LUMO+1 orbitals (d_{XZ}- and d_{YZ}-based orbitals, respectively, in $C_s^{(XZ)}$ symmetry) about the molecular *Z* axis, amounting to a rotation of the principal g_{xx} and g_{zz} directions away from the ideal *XZ* mirror plane.[17] In the case of the high pH form of SO (and very rapid XO), a similar rotation may be a consequence of a "twisting" of the MPT ligand such that the perpendicular of the Mo−S−S plane lies out of the *XZ* pseudomirror plane. Some crystal structures of sulfite oxidase do exhibit such a twisting (e.g., SO with a bound product at the active site: PDB 2A9A), in which instance the fold angle must be considered an average measure; however, it is unclear to what extent this reflects the structure adopted in the Mo^V state in solution. A systematic study of the effects of such twisting on the spin Hamiltonian parameters is beyond the scope of the present study but may offer even more insight into the genuinely triclinic geometry adopted by the active site.

The present work has established that DFT is capable of reasonably reproducing the experimentally observed spin Hamiltonian parameters, as well as estimating the metal−dithiolate fold angle for a well-characterized Mo^V model system. A similar approach could be extended beyond the first-generation model based upon the Tp* ligand to elucidate the geometry of the Mo^V intermediate in mononuclear Mo enzymes with a single MPT ligand by using more relevant structural models of the active site, in particular, replacement of the somewhat inert trispyrazol ligand with more physiological counterparts. By employing the same methodology using crystal structures of XO and SO as starting geometries for DFT-optimization of Mo^V intermediates, the fold angle of the MPT ligand could again be manually varied in order to find the best agreement between the theoretical and experimental **g** and **A**(^{95}Mo) spectroscopic parameters. The effects of changing the degree of "twisting" of the ligand on the low-symmetry EPR parameters could also be further examined. Such considerations represent exciting avenues for future theoretical investigations.

Conclusions

A comparison of the experimental SH parameters of the monoclinic model dithiolene complex Tp*MoO(bdt) with those obtained using DFT analysis of the in vacuo optimized LMoO(bdt) structure shows that the best agreement is

(52) (a) Kisker, C.; Schindelin, H.; Pacheco, A.; Wehbi, W. A.; Garrett, R. M.; Rajagopalan, K. V.; Enemark, J. H.; Rees, D. C. *Cell* **1997**, *91*, 973–983. (b) Schrader, N.; Fischer, K.; Theis, K.; Mendel, R. R.; Schwarz, G.; Kisker, C. *Structure* **2003**, *11*, 1251–1263. (c) Karakas, E.; Wilson, H. L.; Graf, T. N.; Xiang, S.; Jaramillo-Busquets, S.; Rajagopalan, K. V.; Kisker, C. *J. Biol. Chem.* **2005**, *280*, 33506–33515.
(53) Lauher, J. W.; Hoffmann, R. *J. Am. Chem. Soc.* **1976**, *98*, 1729–1742.
(54) Wilson, G. L.; Greenwood, R. J.; Pilbrow, J. R.; Spence, J. T.; Wedd, A. G. *J. Am. Chem. Soc.* **1991**, *113*, 6803–6812.

obtained when the fold angle of this structure is bent to an angle in the vicinity of $\eta \approx 20°$, close to the angle of 21.3° obtained from the X-ray crystallographic structure of Tp*MoO(bdt). Therefore, the theoretical SH parameters of the gas-phase model structure appear useful in extracting geometric information from experimental data, even though this fold angle does not correspond to the global energy minimum ($\eta = 30-40°$). The present results suggest that, provided a reasonable picture of the coordination environment is available from X-ray crystallography and other complementary techniques, a model structure can be built and its Mo^V intermediate then optimized using DFT. Although DFT optimization might not always be capable of accurately predicting the correct geometric structure, especially when a low-energy barrier to a broad range of fold angles exists (Figure 2), we have shown that, by establishing a correlation of the monoclinic SH parameter β with the metal−dithiolate fold angle η of a model complex (Figure 3), information about the geometric structure may be obtained directly from the computer simulation of multifrequency EPR spectra. This is a novel result, because, although it is possible to make a direct connection between the EPR spectrum and the approximate point symmetry at the active site, genuine structural information from empirical simulation of the CW-EPR spectrum of a monomeric Mo^V binding site is often difficult to obtain. We believe our approach of determining the dithiolate fold angle (η) from the non-coincidence angle (β) obtained through computer simulation of multifrequency EPR spectra (required to extract the correct **g** and **A** matrices)[18] will be of immense value in characterizing the geometric and electronic structure of Mo^V species formed during mononuclear molybdenum enzyme catalysis.

Acknowledgment. We thank Prof. Frank Neese, Max Planck Fellow, University of Bonn, for providing the ORCA program. This research was funded in part by the Australian Research Council.

Supporting Information Available: Plot of $d_{x^2-y^2}$ and dithiolate sulfur character of the SOMO as a function of fold angle (Figure S1), principal *g* (Figure S2) and *A* (Figure S3) parameters of the LMoO(bdt) model complex as a function of fold angle, DFT computations of Mulliken charge on the Mo and sulfur atoms and of SOMO ionization energy as a function of fold angle, dependence of the Euler angles on the assignment of the principal directions of **g** and **A**, comparison of the Euler angles corresponding to different permutations of principal values of **g** and **A**, and coordinate files for each of the model structures in XYZ format. This material is available free of charge via the Internet at http://pubs.acs.org.

IC802343F